ADVANCED MATERIALS TECHNOLOGIES
www.advmattechnol.de

Surface-Level Muscle Deformation as a Correlate for Joint Torque

Jonathan T. Alvarez, Ariane de Marcillac, Yichu Jin, Lucas F. Gerez, Oluwaseun A. Araromi, and Conor J. Walsh**

Wearable technology excels in estimating kinematic and physiological data, but estimating biological torques remains an open challenge. Deformation of the skin above contracting muscles—surface-level muscle deformation—has emerged as a promising signal for joint torque estimation. However, a lack of ground-truth measures of surface-level muscle deformation has complicated the evaluation of wearable sensors designed to measure surface-level muscle deformation. A non-contact methodology is proposed for ground-truth measurement of surface-level muscle deformation using a 2D laser profilometer. It shows how three metrics of surface-level muscle deformation—peak radial displacement: $r = 0.94 \pm 0.05$, surface curvature: $r = 0.78 \pm 0.10$, surface strain: $r = 0.83 \pm 0.12$—correlate strongly to changes in volitional elbow torque, further exploring the impact of measurement location or joint angle on these relationships. A nonlinear, lead-lag relationship between surface-level muscle deformation and torque is also found. The findings suggest that surface-level muscle deformation is a promising signal for non-invasive, real-time estimates of torque. By standardizing measurement, the methodology can help inform the design of future wearable sensors.

1. Introduction

Wearable technology has revolutionized the monitoring and quantification of human physiology and movement. From step counts to heart rate and blood oxygen monitoring, wearables have become ubiquitous for capturing both kinematic and physiological data.[1–4]

Despite these advancements, monitoring targeted kinetic information, such as estimating biological joint torque or muscle force remains a challenge. Accurate characterization of muscle loading would yield invaluable insights into biomechanics, robotics, rehabilitation, and sports physiology.[5,6] Joint torque has traditionally been inferred either through musculoskeletal modeling frameworks[7,8] or surface electromyography.[9] However, musculoskeletal modeling is an offline approach that relies heavily on optimization-driven assumptions, and surface electromyography, which measures the electrical activity of a muscle, is neurologically, not mechanically coupled to muscle dynamics.[9,10] In contrast, researchers have identified muscle deformation as a promising candidate signal for joint torque inference, due to its direct coupling to the mechanical output of muscle during a contraction.[11–13]

Muscle deformation, often measured as a change in muscle architecture (e.g., thickness, width, or cross-sectional area), is known to correlate with joint torque.[11,14–16] Ultrasound has been the primary method used to directly measure changes in internal muscle architecture.[17–19] In addition to ultrasound, alternative sensing approaches have focused on surface-level muscle deformation, which is the direct result of internal changes in muscle architecture propagating through soft tissue to the surface of the skin.[20–23] A key advantage of these alternative approaches is greater potential for integration into wearable systems, in contrast to ultrasound which faces challenges related to size and portability constraints. A range of different strategies for monitoring surface-level muscle deformation has been proposed, including multi-sensor force myography.[22,24], localized force myography.[21,25,26], and strain sensing-based myography.[23,27,28] These technologies offer distinct advantages in terms of accessibility, real-time monitoring, cost-effectiveness, and versatility of applications. Additionally, certain sensors can be embedded in a wearable form factor without the need for direct skin contact.[23,29]

Given the multifaceted nature of surface-level muscle deformation, these emerging sensing technologies have been designed to target specific features that result from deformation such as skin strain or changes in curvature. Radial displacement (i.e., normal to the skin surface) above the muscle of interest is another feature of surface-level deformation, however, it cannot be readily measured with wearable devices. True measures of radial displacement require an earth-grounded, stationary system, such as those used in non-contact mechanomyography.[30] or, more commonly, tensiomyography (TMG).[20,31] However, these approaches are limited to 1D, single-point measurements. With no way to decouple the different modes of deformation (e.g.,

J. T. Alvarez, A. de Marcillac, Y. Jin, L. F. Gerez, O. A. Araromi, C. J. Walsh
John A. Paulson School of Engineering and Applied Sciences
Harvard University
Cambridge, MA 02134, USA
E-mail: jonathanalvarez@seas.harvard.edu; walsh@seas.harvard.edu

The ORCID identification number(s) for the author(s) of this article can be found under https://doi.org/10.1002/admt.202400444

DOI: 10.1002/admt.202400444

radial displacement, surface strain, curvature), it is difficult to determine which modes, if any, are most important in influencing the signal transduction of existing wearable deformation sensors. This presents a challenge in both justifying the principles behind existing sensor designs and guiding the development of future wearable devices for estimating joint torque.

The complexity of measuring surface-level muscle deformation underscores the necessity for a consistent and accurate approach to capturing ground-truth measures. In addition, this complexity highlights the need for a systematic experimental framework to understand the relationship between muscle deformation and joint torque across variables known to influence muscle deformation, such as changing joint angles or contraction intensities. Past research has utilized a wide range of external and custom sensors, each with varying mechanical characteristics (e.g., resistive or capacitive, pressure or strain), and behaviors (e.g., linearity, hysteresis, or drift).[22,26,32,33] This has led to a spectrum of models, including linear.[34], curvilinear.[35,36], and cubic.[23] polynomials, have been proposed to define the relationship between surface-level muscle deformation and joint torque. Even in the domain of ultrasound-driven deformation research, where direct and accurate imaging of changes in internal muscle architecture is possible, alternate proposals have suggested linear,[16,37] quadratic,[19] cubic,[18] and even exponential.[38] models to describe the relationship between joint torque and deformation.

When considering how to best translate these insights into practical wearable sensor design, it is crucial that sensors can monitor torque across different muscle loading conditions and joint angles, while also accommodating minor variations in day-to-day placement. This is because muscles can deform not only as a result of a contraction but also as a result of joint kinematic changes. The resting length and tension of muscles are influenced by joint angles. Additionally, joint movement results in a muscle translating longitudinally, shifting the muscle's position parallel to the skin's surface.[15,39] Proximal-distal translation of a muscle can also result from an isometric (fixed-angle) contraction, as the muscle fibers shorten, retracting proximally, and tensioning the distal tendon.[40,41] Previous research has highlighted the effect of changes in joint angle or measurement location on the correlation between deformation and torque.[42] and the range of deformation elicited during a contraction.[43,44] However, these studies only evaluated the correlation for internal deformation of muscle with ultrasound and assessed the range of deformation solely for electrically-elicited contractions at a single point with a displacement sensor. Taken together, changes in the resting length of a muscle and the translation of a muscle underneath the skin are likely to influence both the relationship between surface-level deformation and joint torque and the overall range of induced surface-level deformation during a contraction.

While understanding the shape of the deformation-torque relationship is essential, it is equally important to discern the temporal relationship between these two signals. Early ex vivo experiments on excised soleus muscle from cats observed that radial displacement of the excised muscle led and trailed force changes during the loading and unloading phases of electrically-elicited contractions, respectively.[14,30] TMG researchers reported similar findings in vivo, using a modified instrumented setup to simultaneously log torque and radial displacement during electrically-elicited twitch contractions.[45] Others have also observed an asymmetric relationship between deformation and torque during volitional contractions using ultrasound.[11,18,37] and localized force myographic sensors.[36]; however only qualitative differences were noted. Understanding and quantifying the temporal relationship between deformation and torque can be challenging when using wearable sensors, which are known to have time-dependent non-linearities inherent to the underlying sensing technology. Examples of these non-linearities include stress relaxation or hysteresis in resistive strain and pressure sensors commonly used in the field.[32,33,46] Another important consideration for any muscle sensing modality is muscle fatigue, a time-dependent phenomenon that affects both the amplitude and timing of force production, and often complicates the interpretation of measured signals.[47–49]

The objective of this study was to correlate changes in surface-level muscle deformation with changes in volitionally-generated joint torque using a sensor-agnostic, high-resolution, and non-contact approach. A 2D laser profilometer was used to capture a high-resolution line profile of the skin's surface, measuring micron-scale changes in height relative to the laser head by scanning over a fixed distance and providing detailed height data. Data was collected on the biceps brachii, a primary elbow flexor, during ramped isometric contractions across various elbow angles and measurement locations on the skin's surface. In addition to the peak radial displacement of the limb, measured directly from the laser profiler signal, two additional metrics were calculated: surface curvature, and surface strain, to approximate the types of signals measurable by existing wearable sensors. We also quantified the temporal relationship between joint torque and surface-level deformation. Finally, we investigated the effects of changing joint angles and measurement locations on the range of surface-level muscle deformation.

2. Results and Discussion

In our main experiment, eight healthy individuals (six males, two females; mean ± SD: age: 26.5 ± 2.8 years; height: 1.80 ± 0.07 m; mass: 80.8 ± 17.0 kg; upper arm circumference: 31.8 ± 5.5 cm) performed four ramped, submaximal isometric contractions at three different elbow angles (30°, 60°, 90°) and with the laser profiler focused on three different measurement locations (proximal, center, and distal to the muscle belly) on the surface of the biceps brachii (**Figure 1**; Movie S1, Supporting Information). The laser profiler is a 2D displacement sensor that measures the distance to the surface of the skin across an 8 cm scan line oriented perpendicular to the longitudinal axis of the biceps brachii (transverse anatomical plane) (Figure 1A,B). Reference fiducials were used to ensure consistent alignment for each measurement location, and for all laser profiler data, a second-order polynomial was fit to the data, after removing the corresponding fiducial points (Figure 1C,D). The mean coefficient of determination (r^2) for the quadratic fit was 0.99 ± 0.01, and the root mean squared error (RMSE) between the fit polynomial and raw data was 0.044 ± 0.03 cm. From this polynomial, three surface-level deformation metrics were calculated: peak radial displacement, surface curvature, and surface strain (Figure 1B).

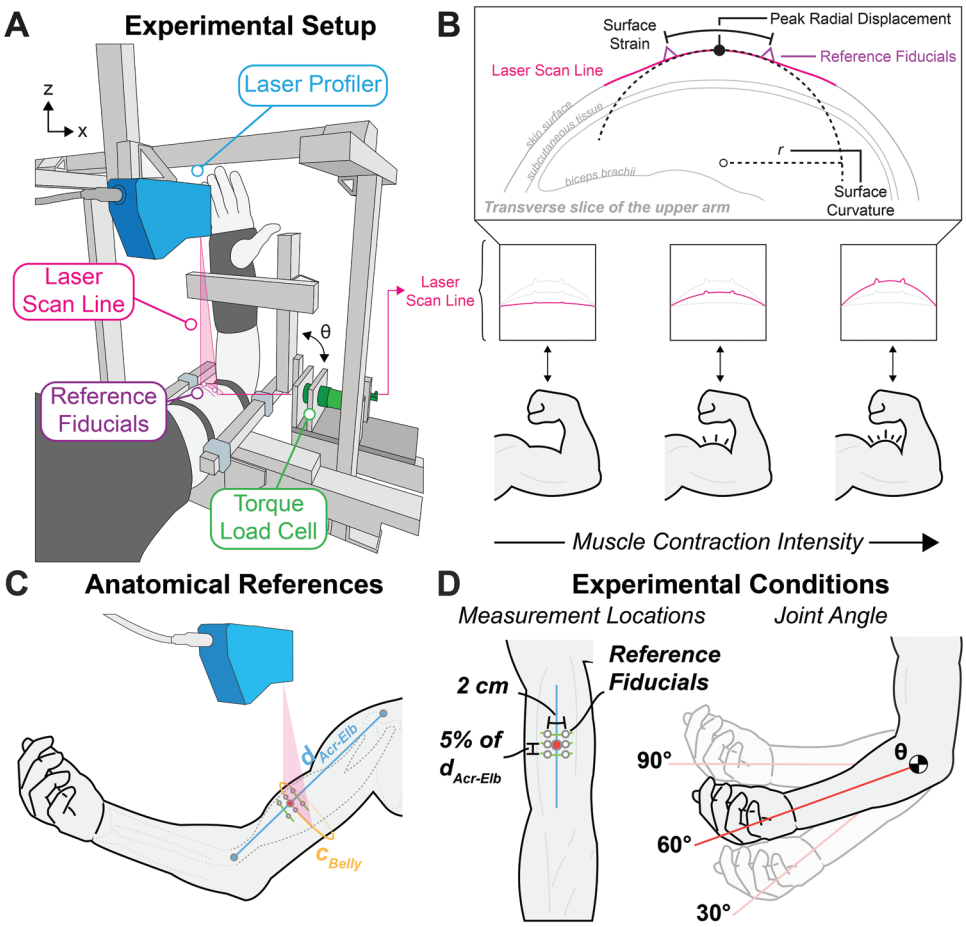

Figure 1. Overview of the experimental setup and derived metrics of surface-level muscle deformation. A) Schematic of the experimental setup. B) Illustration of muscle contraction during a volitional isometric elbow flexion contraction of increasing intensity, with insets depicting raw laser responses (magenta). Expansion callout depicts a transverse slice of the upper arm to illustrate the laser profiler scan line (magenta) and illustrate how each of the metrics of surface-level muscle deformation are derived (black) from the laser data. C) Schematic of anatomical references used to identify measurement locations across participants. D) Overview of experimental conditions: measurement location (distal, center, proximal) and joint angle (30°, 60°, 90°). Note: joint angles were defined relative to full elbow extension (0°).

2.1. Shape of the Relationship between Surface-Level Muscle Deformation and Joint Torque

Several different polynomial and nonlinear fits were evaluated to characterize the overall relationship between joint torque and each metric of surface-level deformation (**Figure 2**; Table S1, Supporting Information). Across all contractions, experimental conditions, and participants, a cubic polynomial yielded the highest mean correlation (r) value for each of the three metrics of surface-level deformation when fitted to joint torque (Table S1, Supporting Information). All correlations presented in the rest of the main text are generated using a cubic fit unless otherwise stated.

2.2. Correlation Between Surface-Level Muscle Deformation and Joint Torque

Peak radial displacement, surface curvature, and surface strain all correlated strongly with joint torque during ramped isometric contractions across all three angles and measurement locations tested (**Figure 3A**). Peak radial displacement correlated most strongly with joint torque ($r = 0.94 \pm 0.05$; RMSE 1.90 ± 1.4 Nm), followed by surface strain ($r = 0.83 \pm 0.12$, RMSE $= 3.09 \pm 1.9$ Nm) and surface curvature ($r = 0.78 \pm 0.10$; RMSE $= 3.63 \pm 2.0$ Nm) across the full contraction cycle. Each contraction can be further segmented into loading, holding, or unloading phases, corresponding to the recruitment, sustainment, and derecruitment patterns of muscle fibers during a contraction. The relative strength of each correlation for these metrics remains consistent across different contraction phases (Table S1, Supporting Information).

2.3. Temporal Relationship between Surface-Level Muscle Deformation and Joint Torque

Peak radial displacement, surface curvature, and surface strain all led and lagged torque production and relaxation as defined by their 50% rise and 50% fall times, respectively (**Figure 4A**).

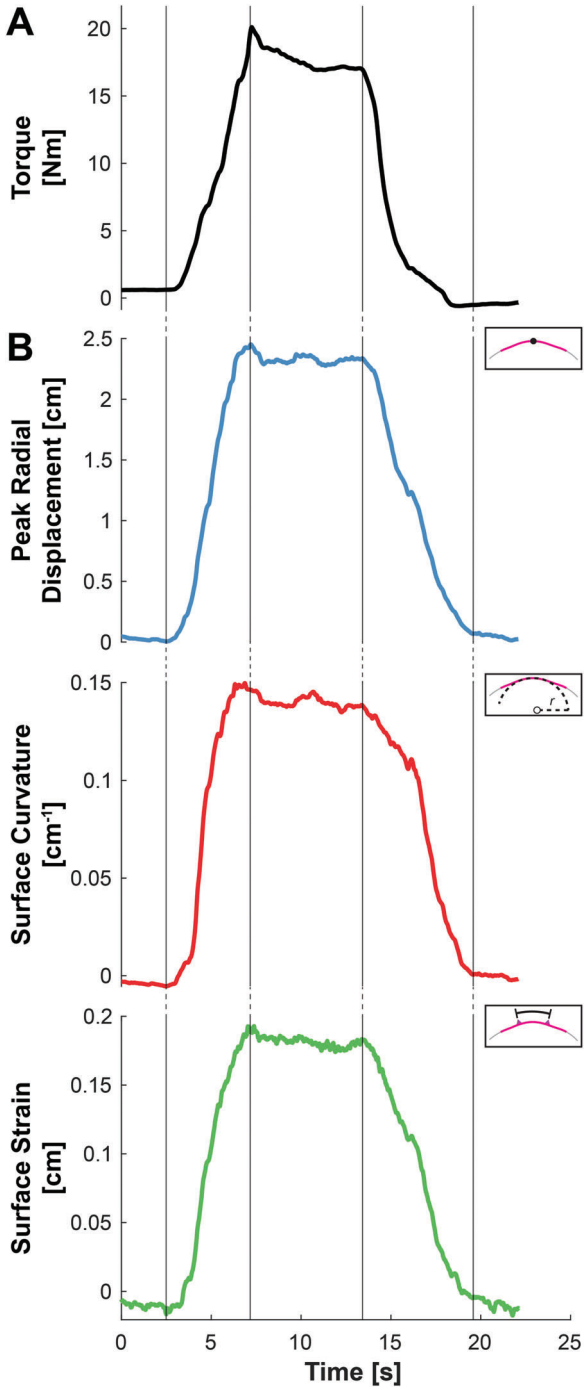

Figure 2. Representative time series data for a volitional contraction illustrate the temporal relationship between A) torque generation and B) surface-level muscle deformation. Vertical lines represent transitions from rest to loading, loading to holding, holding to unloading, and unloading to rest. Insets illustrate how each metric is defined.

During loading, peak radial displacement, surface curvature, and surface strain all led torque generation by an average of 1.67 ± 0.86, 1.90 ± 0.93, and 1.93 ± 0.93 s, respectively. Conversely, during unloading, peak radial displacement, surface curvature, and surface strain lagged torque relaxation by an average of 1.61 ± 1.10, 1.43 ± 2.42, and 0.81 ± 3.14 s, respectively (Figure 4B).

2.4. Effect of Joint Angle and Measurement Location on the Correlation between Surface-Level Muscle Deformation and Joint Torque

The mean correlations between surface-level muscle deformation and elbow joint torque across different joint angles and measurement locations are shown in Figure 3B, Figure S2 (Supporting Information), and summarized in Table S2. There was no statistically significant effect of joint angle on the strength of the correlation between joint torque and peak radial displacement ($F(2,14) = 1.59$, $p > 0.05$) nor surface curvature ($F(2,14) = 0.010$, $p > 0.05$). However, there was a significant effect of joint angle on the strength of the correlation between joint torque and surface strain($F(2,14) = 16.1$, $p < 0.05$). Specifically, the mean correlation strengths at 30° and 60° were both significantly higher than at 90° (30°: $\Delta = 0.109$, $p < 0.05$; 60°: $\Delta = 0.060$, $p < 0.05$). However, there was no statistically significant difference between the mean correlation strengths at 30° and 60° ($\Delta = 0.050$, $p > 0.05$) (Figure 3B).

Measurement location had a similar effect on the correlation strength between each metric and joint torque. As with changes in joint angle, there was no statistically significant effect of measurement location on the strength of the correlation between joint torque and peak radial displacement ($F(2,14) = 1.51$, $p>0.05$) nor surface curvature ($F(2,14) = 0.871$, $p > 0.05$). However, there was a significant effect of measurement location on the strength of the correlation between joint torque and surface strain ($F(2,14) = 12.7$, $p < 0.01$). Specifically, the mean correlation strength for the distal location was significantly less than the proximal location ($\Delta = -0.143$, $p < 0.05$), but did not significantly differ from the center location ($\Delta = -0.080$, $p > 0.05$). There was no significant difference in mean correlation strength between the center and proximal locations ($\Delta = -0.064$, $p > 0.05$) (Figure 3B).

2.5. Effect of Joint Angle and Measurement Location on the Range of Surface-Level Muscle Deformation

For all participants, angles, and measurement locations, the range of deformation for each metric was calculated as the difference between the maximum and minimum value observed within a single contraction. To facilitate inter-participant comparisons, these ranges were normalized by the maximum range of deformation observed for each metric per participant (**Figure 5**; Figure S3, and Table S3, Supporting Information).

The results did not reveal a significant effect of joint angle on the normalized range of surface curvature ($F(2,14) = 0.273$, $p > 0.05$) or surface strain ($F(2,14) = 2.786$, $p > 0.05$) (Figure 5A). However, there was a significant effect of joint angle on the normalized range of peak radial displacement ($F(2, 14) = 7.42$, $p < 0.01$). The mean normalized range of displacement at 30° was significantly less than at 90° ($\Delta = -0.178$, $p < 0.01$), but was not different from 60° ($\Delta = -0.091$, $p > 0.05$). There was no statistically significant difference between 60° and 90° ($\Delta = -0.087$, $p > 0.05$).

Measurement location had a more pronounced effect on the range of deformation (Figure 5B). The analysis revealed a significant effect of measurement location on the normalized range

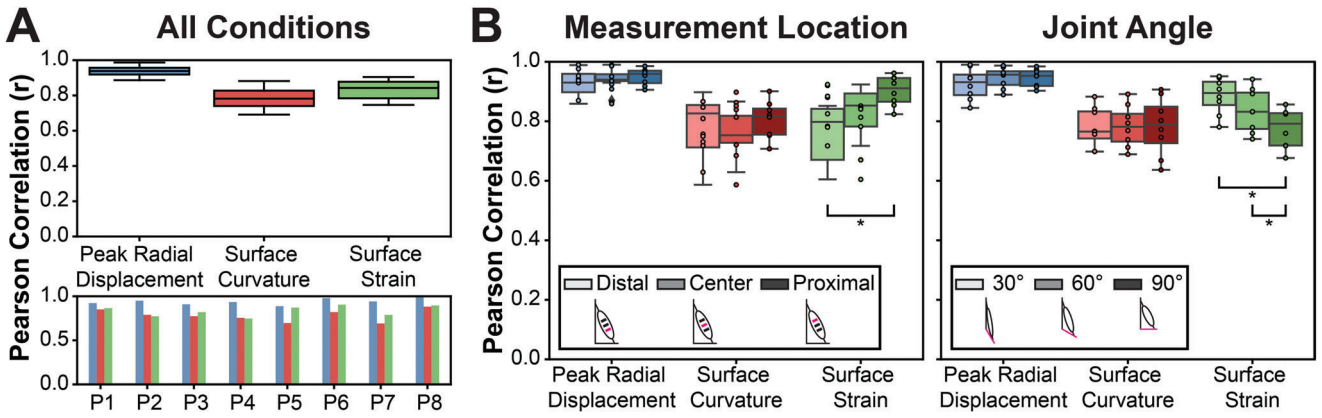

Figure 3. Correlation between metrics of surface-level muscle deformation and joint torque for eight participants. A) Overall correlation between each of the surface-level muscle deformation metrics and joint torque across all participants and all experiments. Grouped bar plots depict individual correlation values for each metric per participant. B) Correlation between each metric of surface-level muscle deformation and joint torque, grouped by experimental conditions; colored dots represent the mean per participant and black dots represent outliers. *Indicates statistically significant mean differences between conditions (determined via repeated-measures ANOVA and post hoc Bonferroni method, $p < 0.05$).

of both peak radial displacement ($F(2,14) = 38.6$, $p < 0.001$) and surface strain ($F(2,14) = 50.5$, $p < 0.001$), but not surface curvature ($F(2,14) = 1.97$, $p > 0.05$). For peak radial displacement, the normalized range varied across all measurement locations, increasing from distal to proximal (Distal – Center: $\Delta = -0.170$, $p < 0.01$; Distal – Proximal: $\Delta = -0.268$, $p < 0.01$; Center – Proximal: $\Delta = -0.098$, $p < 0.001$). Similarly, for surface strain, the normalized range also varied across all measurement locations, increasing from distal to proximal (Distal – Center: $\Delta = -0.205$, $p < 0.01$; Distal – Proximal: -0.310, $p < 0.01$; Center – Proximal: $\Delta = -0.104$, $p < 0.001$).

3. Discussion

Deformation of the skin above a contracting muscle is a promising candidate signal for tracking changes in joint torque. In this work, we present a new methodology that enables a systematic characterization of the relationship between surface-level

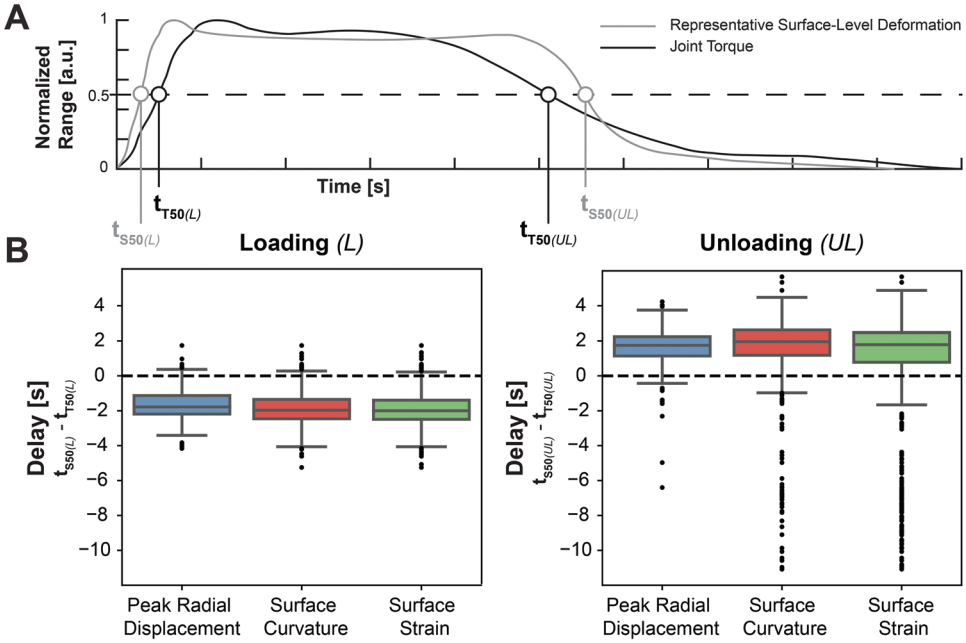

Figure 4. Temporal relationship between surface-level muscle deformation metrics and joint torque, as defined by the difference between the 50% rise and 50% fall time, across all experimental conditions and participants. A) Exemplar data to illustrate the identification of temporal parameters using the 50% rise and 50% fall times of surface-level muscle deformation metrics and joint torque. B) Time difference between each deformation metric and joint torque during loading and unloading calculated for each contraction; black dots represent outliers. A dashed line denotes no time difference. A negative time difference during loading indicates that the skin deforms prior to joint torque generation, whereas a positive time difference during unloading indicates that deformation lags torque relaxation.

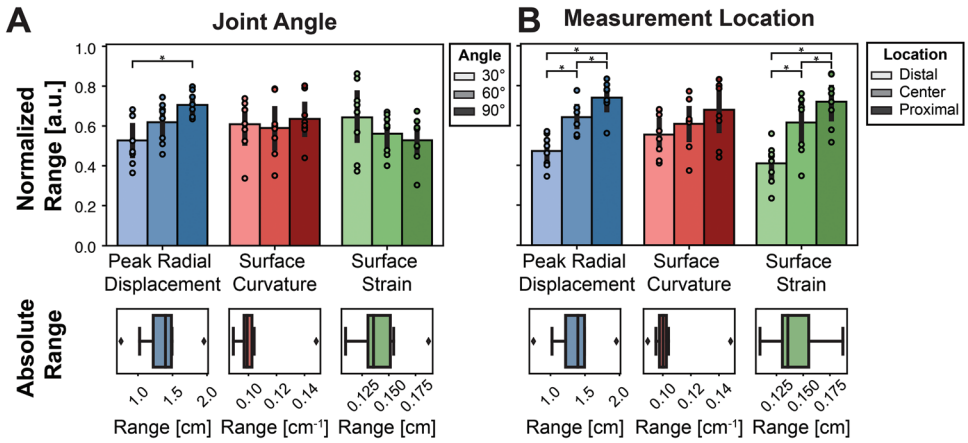

Figure 5. Range of surface-level muscle deformation induced during a volitional contraction across conditions. A) Bar plots depict the normalized range of each surface-level deformation metric grouped by joint angle or measurement location for eight participants; colored dots represent the mean per participant. B) Absolute range of each metric in standardized units of distance for all participants; black dots represent outliers. *Indicates statistically significant mean differences between conditions (determined via repeated-measures ANOVA and post hoc Bonferroni method, $p < 0.05$).

deformation (of the skin of the upper arm) and volitionally-generated torque at the elbow during isometric contractions, across different elbow angles and measurement locations. The proposed non-contact methodology (utilizing a laser profilometer) provides high-resolution measurements (<10 μm) while remaining immune to the inherent non-linearities of existing wearable sensors, enabling sensor-agnostic measurements of deformation at the skin's surface. Additionally, our approach allows for concurrent measurement of volitionally-generated joint torque alongside a two-dimensional measure of surface-level deformation, enabling the extraction of metrics other than peak radial displacement: surface curvature and surface strain.

Across all joint angles and measurement locations, the average correlation coefficients for a cubic polynomial model revealed that surface-level deformation correlated strongly with elbow flexion joint torque during the full contraction cycle. Specifically, peak radial displacement exhibited the strongest average correlation with joint torque ($r = 0.94 \pm 0.05$), followed by surface strain ($r = 0.83 \pm 0.12$), and surface curvature ($r = 0.78 \pm 0.10$) (Figure 3A). Although we cannot directly compare our results to existing studies in literature, we can compare them to those using ultrasound imaging to monitor deformation of the elbow flexors as reference. Shi et al. (2008) reported a linear correlation coefficient of $r = 0.93 \pm 0.22$ between ultrasound-derived biceps brachii thickness and elbow torque during only the loading phase of isometric contractions at 90° elbow flexion.[17] Similarly, Hallock et al., (2020), reported a linear correlation coefficient of $r = 0.67 \pm 0.16$ for changes in brachioradialis thickness compared to torque using ultrasound during isometric contractions across a range of five elbow angles.[16]

A key finding of our work was that a cubic fit, with a correlation range across all metrics of $r = 0.78$–0.94, provided the strongest correlation between surface-level deformation and joint torque over the full contraction cycle, as compared to linear ($r = 0.65$–0.88), quadratic ($r = 0.74$–0.93), or exponential ($r = 0.63$–0.84) fits which are commonly reported in the literature (Table S1, Supporting Information). Considering the physiology of muscle contractions, a cubic relationship is consistent with three distinct regions that describe the relationship between deformation and force. During loading, as a muscle begins to contract and apply force, muscle fibers shorten to take up slack in the tendon, resulting in large changes in muscle architecture at low forces. At moderate forces, tension is efficiently transmitted from the muscle through the tendon as both tendon stiffness and muscle force increase proportionally. Finally, at high forces, the muscle-tendon unit is close to full elongation, resulting in less change in muscle deformation for a given unit change in muscle force.[11,15,30,40] During unloading, the same explanation holds, just in reverse, leading to the observed lead-lag phenomena, whereby joint torque is higher during unloading for a given surface-level deformation metric compared to loading. This also highlights the impact of the tendon, where elastic energy stored during contraction is released during relaxation, enabling sarcomeres to return to their resting state more quickly.[45,50] The curvilinear relationship between deformation and joint torque is likely influenced by muscle type (pennate vs parallel), specific joint constraints (isometric vs isotonic), contraction type (volitional vs electrically-elicited), and contraction length.[11] Discrepancies between our results and those from previous studies could arise from variations in these experimental parameters. For example, a prior study that used a modified TMG setup with low amplitude and short-duration electrical stimulation used a quadratic fit to describe the relationship between peak twitch torque amplitude and radial displacement.[35] It is possible that the discrepancy between their cited fit and our own is that a single electrically-elicited twitch contraction failed to generate sufficient force to fully elongate the muscle-tendon unit.[51] The discrepancy may also result due to a difference in muscle fiber recruitment between electrically-elicited and volitional contractions.[52]

A cubic relationship between surface-level deformation and joint torque also agrees well with our observation that the rate of deformation leads the rate of force production during loading but lags force production during unloading (Figure 4B). All features of surface-level deformation consistently led torque production and lagged torque relaxation during

volitional contractions, in line with previous findings from electrically-elicited contractions measured with TMG.[35,45] and surface mechanomyography.[14,30], as well as observations from ultrasound.[18,37] Previous research suggests part of the observed lead-lag phenomena may be exacerbated by the measurement of torque with an external transducer, where the force exerted by a contracting muscle must first propagate through connective tissue before registering as a mechanical load on the transducer.[35,45] However, the precise magnitude of this effect remains uncertain without direct measurements of muscle force, which necessitate invasive procedures.[53–55] Regardless, it is clear that deformation propagated to the skin occurs prior to full propagation of force to the joint. Using a non-contact optical laser to measure and understand these temporal dynamics helps isolate true underlying physiological deformation from sensor-related non-linearities, preserving the true deformation signal which has been shown to reflect fatigue.[23,56,57], damage.[49], or composition.[58,59]

Across all three elbow angles and measurement locations, peak radial displacement and surface curvature consistently exhibited strong correlations with joint torque (Figure 3B). Conversely, the correlation between surface strain and joint torque was significantly influenced by changes in both joint angle and measurement location (Figure 3B). Prior studies have acknowledged an effect of joint angle on the deformation-torque relationship, albeit on different muscles and different metrics of deformation.[16,19] Additionally, although prior research utilizing ultrasound imaging has shown variations in the biceps brachii's cross-sectional area and thickness along its proximal-distal axis.[42], the extent to which measurement location influenced the deformation-torque relationship during voluntary contractions had yet to be fully explored.

While it's important to examine how joint angle or measurement location influences the correlation between deformation and torque, it's equally valuable to understand their effect on the amount of deformation induced during a contraction. Insights into the range of deformation can help inform the resolution and sensitivity requirements for future wearable devices. Our data agree with previous findings from TMG literature which demonstrated a significant effect of joint angle.[43] and measurement location.[41,44] on the magnitude of radial displacement elicited by electrical stimulation. Our results confirm and extend these findings for volitional contractions and simulated wearable metrics (surface curvature and strain) (Figure 5A,B). The normalized range of peak radial displacement increased significantly with increased joint flexion and a more proximal measurement location. A mirrored effect was observed for surface strain where the range of surface strain increased the more proximal the measurement location. Interestingly, the range of surface curvature was not significantly altered by changes in joint angle or measurement location.

Collectively, this data reveals a clear impact of joint angle on the correlation between surface strain and joint torque and the range of peak radial displacement. The data also reveal how changing measurement locations affect the correlation between surface strain and joint torque and the range of both peak radial displacement and surface strain, underscoring the importance of sensor placement in wearables. However, crucially, neither joint angle nor measurement location had a statistically significant effect ($p > 0.05$) on the strength of the correlation nor range of surface curvature. Notably, the differences for each deformation metric were maximized at the extremes of both the range of motion (30° vs 90°) and measurement locations (distal vs proximal) (Figures 3B and 5). We hypothesize that these effects are mediated primarily by underlying muscle translation and associated changes in compliance of the muscle-tendon unit. Passive translation during joint rotation results in the muscle belly shifting distally at 30° compared to 90° as the muscle is passively lengthened.[15,39] Active translation during a concentric contraction results in proximal translation of the muscle belly, caused by the muscle shortening and tensioning the distal tendon.[40,41] Support for this hypothesis is evident in the peak radial displacement signal, which showed the largest range at 90° (Figure 5A), consistent with increased radial bulging from greater sarcomere shortening and an enhanced resting cross-sectional area of the underlying muscle at 90°. Conversely, the range of peak radial displacement was minimized at extended elbow angles (Figure 5A), consistent with overextended sarcomeres and an increase in the stiffness of the elastic component of the muscle-tendon unit.[43]

Although peak radial displacement consistently demonstrated the highest correlations with joint torque across all angles and measurement locations (Figure 3), monitoring changes in surface curvature appears to be a promising approach for wearable sensing moving forward. Unlike peak radial displacement, the range of surface curvature was not significantly affected by changes in joint angle or measurement location (Figure 5). Coupled with consistent correlations across joint angles and measurement locations, this robustness in the surface curvature magnitude response underscores a crucial advantage for real-world applications. It ensures reliable joint torque estimation across a spectrum of dynamic activities, where joint angles are not static, increasing the practical utility of using surface-level muscle deformation in variable everyday conditions. Moreover, surface curvature is readily measurable with existing wearable sensing technology.[23,60–62] In contrast, although there is growing research investigating alternative approaches sensitive to peak radial displacement.[63], their reliability is difficult to quantify, due to challenges such as maintaining consistent reaction forces or isolating sensors from mechanical coupling effects.[26,33] As for surface strain, although, like surface curvature, it can be easily measured with current wearable sensing technology, its high sensitivity, in both correlation and range, to variations in joint angle or measurement location (Figures 3B and 5) may limit its practicality in future wearables based on our findings.

Sensor placement remains an important consideration, as evidenced by the significant effect of measurement location on the correlation strength of surface strain and the range of peak radial displacement and surface strain (Figure 5B). This variability highlights the potential importance of establishing a calibration procedure (or more advanced algorithmic intervention) following doff and don cycles to maintain estimation accuracy with variations in sensor placement. Notably, the range of surface curvature response did not exhibit statistically significant differences across measurement locations (Figure 5B), and therefore minor variations in placement may not markedly influence the response. However, non-significant trends for surface curvature do suggest more testing should be performed to both confirm these results

and possibly identify the limit of insensitivity to placement for each metric.

Taken together, while surface curvature appears promising for estimating joint torque, increasing sensor coverage with multiple deformation sensors or integrating different sensing modalities may help improve estimation accuracy. It is possible that using multiple curvature sensors could capture a richer dataset from the underlying muscle deformation, and further improve correlation strength across conditions.[64] In addition, multiple sensors could also be useful for mitigating sensor placement sensitivity by using relative changes between sensors to recalibrate after each don.[24] Additionally, although not statistically significant, changes in joint angle did influence the correlation and range of surface curvature. Therefore, fusing additional sensing modalities, such as inertial measurement units, to capture changes in joint angle could help bolster signal robustness during dynamic movements.[65,66] Lastly, because surface-level deformation is a measure of the mechanical output of muscle, incorporating a measure of the (neural) electrical input to muscle with electromyography may improve the characterization of the underlying muscle physiology.[26,67,68] and could assist with suppressing motion artifacts by gating signals based on muscle activity.[69] While the above considerations focus on surface curvature, it's crucial to note that the same principles and recommendations also extend to sensors measuring other modes of deformation.

3.1. Limitations

Although this work demonstrated promising results, it is important to acknowledge certain limitations that warrant further investigation. First, all of the participants tested in this study were healthy, young adults (<35) who self-reported as moderate to highly active. We hypothesize that the relationships described between surface-level deformation and joint torque may change in less active, aging, or clinical populations where there may be higher contents of subcutaneous fat or less baseline muscle mass.[70,71] Second, only a single, parallel muscle, the biceps brachii, was evaluated under isometric conditions for this work. Different fiber orientations in muscle, such as the angled muscle fibers of pennate muscle, have different gearing patterns during a contraction, which may influence the underlying relationship between deformation and torque.[72,73] Additionally, further research is needed to determine if surface muscle deformation ever reaches a saturation point.[11,74] Third, all of the contractions in this work were slow, prescribed, submaximal (≤50%) isometric contractions. Recognizing the constraints imposed by the static positioning of the arm during isometric contractions, future research is needed to explore the relationship between muscle deformation and output joint torque across a broader spectrum of conditions. This includes examining more varied contraction types (e.g., isotonic and isokinetic), contraction speeds, and contraction intensities to expand the applicability and practicality of using surface-level muscle deformation to estimate joint torque in real-world scenarios. Fourth, while we focused this work on the correlation between surface-level deformation and joint torque, further investigation is needed to understand how deformation signals can be used to predict absolute values of torque during a contraction. Finally, expanding our investigation to include both non-transverse plane deformation and multidimensional deformations (e.g., joint torsion) would further enhance our understanding of surface-level muscle deformation and its relationship with joint torque.

4. Conclusion

Our study introduces a new, standardized methodology to accurately characterize the relationship between surface-level deformation and joint torque using a non-contact laser profilometer. With this approach, we can directly measure peak radial displacement and derive surface curvature and surface strain. Our results show that peak radial displacement, surface curvature, and surface strain all correlate strongly with elbow flexion joint torque across a range of elbow angles and measurement locations (Figure 3). We also found that surface-level deformation leads and lags torque during a volitional contraction (Figure 4B), in agreement with a cubic deformation-torque relationship, and in line with previous research using electrically-elicited contractions and observations from ultrasound. Unlike peak radial displacement and surface strain, surface curvature was not significantly affected by changes in joint angle or measurement location (Figures 3B and 5), exhibiting strong and consistent correlations with joint torque and range of responses across all conditions, underscoring its potential for future wearable approaches during dynamic activities. However, surface curvature also had the lowest overall mean correlation with joint torque across all conditions, so leveraging combinations of metrics may offer a promising research direction moving forward. This research represents an essential step toward a systematic examination of how surface-level deformation and its derivatives can inform joint torque estimation. Accurate joint torque estimation has wide-ranging applications, such as monitoring the rehabilitation progress of patients recovering from musculoskeletal injuries, enabling adaptive control of assistive exoskeletons, or optimizing training and injury prevention protocols in competitive sports by accurately assessing muscle load and fatigue. Moving forward, studies should prioritize on-body calibration to address variability in the range of deformation due to sensor placement and consider fusing additional sensing modalities for capturing joint angles.

5. Experimental Section

Keyence LJ-X8200 Laser: A laser profiler (LJ-X8200, Keyence Inc.) was used as a ground-truth measure of surface-level deformation. The laser profiler is a 2D displacement sensor that measures the distance to a target (z-axis resolution: 1 µm ± 300 nm) across an 8 cm scan line. The laser provides repeatability of 3 µm on the x-axis and 1 µm on the z-axis, linearity of ± 0.03% of full scale (full scale = 41 mm), and a scan range of ± 34 mm centered around a depth of 245 mm. Data was collected along the scan line at 25 µm increments (3200 points). During the experiment the laser profiler was mounted to an adjustable 3-axis gantry to align the visible scan line to a predetermined measurement location (see *Participant Preparation*) on the surface of the skin (Figure 1A). The setup ensured the device was always oriented to scan perpendicular to the long axis of the biceps brachii, along the transverse anatomical plane. All 3200 points of laser data were sampled every 10 ms (100 Hz); each point representing raw height data measured between the surface of the skin

and the scanning head (Figure 1A,B). For all experiments, participants donned laser-safe goggles (KBS-5305, Kentek Corporation).

Benchtop Setup: A benchtop setup was designed to measure elbow flexion torque and assist with alignment of the laser profiler to the participant (Figure 1A). Elbow flexion torque was measured as a proxy for muscle force as it is not possible to directly and non-invasively measure forces from individual muscles.[8] The setup consisted of an angle-adjustable lever arm to measure elbow joint torque, a set of arm supports to support and restrain the upper arm during testing, and a 3-axis gantry to align and adjust the laser profiler to the upper arm.

The lever arm was constructed from aluminum extrusions (80-20, 80-20 LLC.) with foam supports and a wrist strap at one end to secure the participant's wrist. The other end of the lever arm was secured to a reaction torque load cell (TTF-350; Futek Inc.) with a range of 145 Nm. This load cell was mounted on a rotatable plate, adjustable in 15-degree increments, facilitating quick and precise elbow angle adjustments during testing. The arm supports consisted of two 3D-printed semicircular cuffs designed to slide along aluminum extrusions for alignment to the olecranal region near the elbow and the axillary region just distal to the armpit. Foam inserts were attached to each cuff, and adjustable straps were provided to secure the upper arm in place, preventing unwanted shoulder flexion during contractions. The 3-axis gantry was also made from aluminum extrusions and enabled precise alignment of the laser profiler to each participant's unique anatomy in all anatomical planes.

Participants: Eight healthy participants (six males, two females; mean ± SD: age: 26.5 ± 2.8 years; height: 1.80 ± 0.07 m; mass: 80.8 ± 17.0 kg; upper arm circumference: 31.8 ± 5.5 cm) were recruited to participate in the experimental protocol. All participants self-reported as active individuals and the right arm was evaluated, regardless of dominance. All participants consented prior to participation in the protocol, which was approved under protocol IRB17-1201 by the Harvard Medical School Institutional Review Board.

Participant Preparation: Upon arrival at the laboratory, participants were given an overview of the experimental protocol and then led through a series of static and dynamic warm-up stretches of the upper arm. Next, participants were seated and asked to fully extend their elbows. A line was drawn with a skin-safe marker along the axis defined by the acromion and the cubital fossa (elbow pit), just proximal to the distal insertion of the bicep's tendon. The total length of this axis was denoted $d_{acr\text{-}elb}$. The participant was then asked to flex their elbow at 90° and the most prominent point of the biceps brachii (the muscle bulge peak) was visually identified by the research team and marked. The circumference of the upper arm passing through this point was denoted c_{belly} (Figure 1C).

Three locations were defined relative to these anatomical measurements: the center was centered at the belly peak (c_{belly}), and the proximal and distal locations were marked at points 5% of the $d_{acr\text{-}elb}$ distance proximal or distal of the center location, respectively (Figure 1D). Each was marked on the surface of the skin with a 4 cm line drawn perpendicular to the acromion-elbow axis. Finally, two points were marked 1 cm on either side of the acromion-elbow axis along the three transverse lines delineating each of the three measurement locations. These two points were used to place custom 3D-printed fiducial markers, which enabled accurate registration of the laser profiler to the marked measurement locations (Figure 1B,D). Therefore, during data collection, any misalignment between the measurement location and visible scan line of the laser profiler would manifest as an absence of one or both fiducial reference markers on the output signal. If a misalignment occurred for more than 0.5s, that contraction was repeated.

Following anatomical measurements and placement of the fiducial markers, participants were guided to the benchtop setup. The lever arm was adjusted to position the crossbar on the anterior aspect of the distal forearm, just proximal to the wrist joint. To prevent unwanted wrist flexion or extension, participants donned a wrist brace for the remainder of the study.[16] Each participant's upper arm was then secured with strapping to the two upper arm supports to prevent shoulder flexion and minimize movement. Finally, the participants donned the laser-safe goggles.

Experimental Protocol: The experimental protocol was designed to measure biceps brachii contraction-induced changes in surface-level deformation of the upper arm along the transverse plane at three different elbow angles (30, 60, and 90°), three different measurement locations (proximal, center, and distal to the muscle belly), and two different contraction intensities (25% and 50% MVIC) (Figure 1D). Note, that joint angles were calculated relative to full elbow extension (0°). The experimental protocol consisted of two experiments: a set of baseline maximum voluntary isometric contractions (MVIC) at varying angles (baseline collection) and a sweep of submaximal ramped isometric contractions at varying angles with the laser profiler focused on each of the three measurement locations (experimental sweep) (Figure S1, Supporting Information).

Experimental Protocol:Baseline Collection: Participants were instructed to complete three MVICs at each of the three elbow angles (30, 60, and 90°). One minute rest was provided after each contraction. Following each set of three MVICs, the research team adjusted the angle of the lever arm. Participant MVICs were collected at all three elbow angles to account for the impact of joint angle and resting muscle length on the maximum force-generating ability of a muscle.[75]

Experimental Protocol:Experimental Sweep: For each elbow angle (30, 60, and 90°) and measurement location (distal, center, proximal) participants completed four ramped submaximal isometric contractions. Submaximal contractions were performed to minimize the effects of fatigue. Each ramped isometric contraction consisted of a five-second ramp from rest to the target %MVIC (loading phase), a five-second hold at the target %MVIC (holding phase), and a five-second ramp down to rest (unloading phase) (Figure S1, Supporting Information). The target torque for the first two contractions was defined as 50% of the participant's MVIC at the current angle being tested. The target torque for the following two contractions was defined as 25% of the participant's MVIC at 90°. The contractions at 50% MVIC facilitated comparisons across the range of motion based on the bicep brachii's relative force-generating capacity at a specific joint angle and resting length. In contrast, the 25% MVIC contractions provided a standardized comparison to an absolute value of torque, independent of joint angle and its impact on the bicep brachii's force-producing capability.

The experimental protocol was grouped by measurement location. For each measurement location, all three angles were assessed prior to advancing to the next measurement location. To mitigate fatigue, participants were given a minimum rest of 15 s between contractions, 1 minute between elbow angles, and 5 min between measurement locations. The laser profiler emits a visible scan line along its measurement axis. Participants were instructed to ensure this visible scan line bisected both fiducials throughout the duration of each ramped isometric contraction. If a misalignment between the laser scan line and the measurement location occurred during a contraction for more than 0.5 s, that contraction was repeated. Audio feedback with the current torque was provided every second for the participants in order to complete each ramped isometric contraction to the desired target torque value.

Data Processing: Raw data from the laser profiler was sampled at 100 Hz through LJ-X Navigator (v1.03.00, Keyence). Raw data from the torque load cell was conditioned with a strain gauge analog amplifier (IAA100, Futek Inc.) and then sampled at 1 kHz with a PowerLab 8/35 (AD Instruments) external data acquisition unit (DAQ). An external trigger signal was sent from the DAQ to the laser profiler controller (LJ-X8000A, Keyence) at the onset of data logging to synchronize both data streams.

Data Processing:Baseline Collection: The maximum torque generated across all three MVICs per elbow angle was extracted. The maximum torque generated per angle was then used to calculate the 50% and 25% torque targets used in the Experimental Sweep.

Data Processing:Experimental Sweep: To ensure proper collocation of the laser profiler scan line and the sensing location, all raw laser data was first processed to ensure both fiducials were present in the signal. If, for any frame, one or both fiducials are missing, that frame's data was replaced with the preceding frame's data, provided the preceding frame was not an outlier. After this pre-processing step, the location of the fiducials was recorded and the points on the raw laser signal corresponding to the fiducials were removed. Finally, for all frames, a second-order polynomial was fit to the pre-processed laser profiler data. A polynomial function was fit to the raw data as a polynomial is

analytically differentiable, which facilitated further analysis. From this polynomial, all three of the surface-level deformation metrics were calculated (Figure 1B).

For all contractions, the start, end, and transitions (from loading to holding and holding to unloading) were manually identified and recorded by the research team. To quantify the temporal relationship between surface-level deformation and joint torque, the 50% rise and fall time of each metric relative to joint torque was calculated.[76] To determine the relationship between surface-level deformation and joint torque, the Pearson correlation coefficient (r) and root mean squared error (RMSE) were calculated between each of the three metrics and joint torque for every contraction. Correlations were calculated across the entire ramped isometric contraction, as well as for the loading, holding, and unloading stages of the contraction (Figure 3A; Table S1, Supporting Information). For comparison, the correlations were calculated across four different models: linear, quadratic, cubic, and second-order exponential. To assess the impact of joint angle or measurement location on the range of surface-level deformation, the normalized range for each metric was calculated. Only the 25% MVIC contractions were used to calculate the normalized range per metric because of the standardized torque target across all angles. For each contraction, both the deformation metrics and joint torque were segmented, and the difference between their minimum and maximum values was computed (Figure 5A,B). These differences were normalized to the greatest difference observed for any contraction within an individual participant (Figure 5C). It was noted that data from one trial for one participant was missing (proximal measurement location at elbow angle of 90°) due to technical issues with the laser system software during collection.

Surface-Level Muscle Deformation Metrics: Peak radial displacement was defined as the minimum distance between the surface of the skin and the laser profiler head and was calculated as the maximum height of the derived polynomial, $f(x)$, per frame. Surface curvature was defined as the maximum curvature of the surface of the skin along the transverse plane. Surface curvature was derived using the following formula for calculating the curvature of planar curves.[77]

$$k(x) = \frac{f''(x)}{\left(1 + f'(x)^2\right)^{\frac{3}{2}}} \quad (1)$$

where surface curvature was defined as the maximum of $k(x)$ per frame. Surface strain was defined as the distance along the surface of the skin, the arc length, between the two fiducials per frame. To calculate arc length of $f(x)$, the linear chordal approximation was used to approximate the arc length between each point along the surface of the skin between both fiducials.[78]

Statistics: Statistical analyses were performed using R.[79] A repeated-measures Analysis of Variance (ANOVA) was used to compare the strength of the correlation coefficients for the three metrics across varying elbow angles or measurement locations. Where the F-ratio was found to be significant for the effect of joint angle or measurement location on the strength of a metric's correlation coefficient, post-hoc analyses with a Bonferroni adjustment were used to assess between which angles or locations a significant difference existed. Repeated-measures ANOVA was also used to compare the normalized range of deformation change of each metric across varying elbow angles or measurement locations. Where a significant F-ratio was found, post-hoc analyses with Bonferroni adjustment were used for all pairwise comparisons. Further statistical tests assessing the reliability of our data collection methods are detailed in the *Supporting Information*. All data are presented as mean ± standard deviation in the text unless otherwise stated.

Supporting Information

Supporting Information is available from the Wiley Online Library or from the author.

Acknowledgements

The authors acknowledge funding from the National Science Foundation (NSF DARE Award #2019621), and support from the John A. Paulson School of Engineering and Applied Sciences at Harvard. The authors would also like to thank Mollie Ebeling, Philipp Arens, David Adam Quirk, Lauren Baker, and Benjamin Sibson for advice on illustrations and statistical analysis, Krithika Swaminathan and David Farrell for their insights and assistance during the review process, and the Wyss Institute Clinical Research Team for their help with the development of the study protocol.

Conflict of Interest

The authors declare no conflict of interest.

Data Availability Statement

The data that support the findings of this study are available on request from the corresponding author. The data are not publicly available due to privacy or ethical restrictions.

Keywords

joint torque, muscle deformation, wearable sensors

Received: April 16, 2024
Published online:

[1] J. Heikenfeld, A. Jajack, J. Rogers, P. Gutruf, L. Tian, T. Pan, R. Li, M. Khine, J. Kim, J. Wang, J. Kim, *Lab Chip* **2018**, *18*, 217.
[2] (Ed., E. Sazonov), *Wearable Sensors: Fundamentals, Implementation and Applications*, 2nd ed, Elsevier Science, Amsterdam, Netherlands **2020**.
[3] S. Majumder, T. Mondal, M. J. Deen, *Sensors* **2017**, *17*, 130.
[4] T. R. Ray, J. Choi, A. J. Bandodkar, S. Krishnan, P. Gutruf, L. Tian, R. Ghaffari, J. A. Rogers, *Chem. Rev.* **2019**, *119*, 5461.
[5] P. G. Adamczyk, S. E. Harper, A. J. Reiter, R. A. Roembke, Y. Wang, K. M. Nichols, D. G. Thelen, *Curr. Opin. Biomed. Eng.* **2023**, *28*, 100492.
[6] F. Porciuncula, A. V. Roto, D. Kumar, I. Davis, S. Roy, C. J. Walsh, L. N. Awad, *PM&R* **2018**, *10*, S220.
[7] S. L. Delp, F. C. Anderson, A. S. Arnold, P. Loan, A. Habib, C. T. John, E. Guendelman, D. G. Thelen, *IEEE Trans. Biomed. Eng.* **2007**, *54*, 1940.
[8] A. Erdemir, S. McLean, W. Herzog, A. J. van den Bogert, *Clin. Biomech.* **2007**, *22*, 131.
[9] T. J. Roberts, A. M. Gabaldón, *Integr. Comp. Biol.* **2008**, *48*, 312.
[10] C. Disselhorst-Klug, T. Schmitz-Rode, G. Rau, *Clin. Biomech.* **2009**, *24*, 225.
[11] P. W. Hodges, L. H. M. Pengel, R. D. Herbert, S. C. Gandevia, *Muscle Nerve* **2003**, *27*, 682.
[12] Y. Zhou, YP. Zheng, S. Bioeng, *Sonomyography Dynamic and Functional Assessment of Muscle Using Ultrasound Imaging*, Springer, **2021**, https://link.springer.com/book/10.1007/978-981-16-7140-1.
[13] T. J. Roberts, C. M. Eng, D. A. Sleboda, N. C. Holt, E. L. Brainerd, K. K. Stover, R. L. Marsh, E. Azizi, *Physiology* **2019**, *34*, 402.
[14] C. Orizio, R. V. Baratta, B. H. Zhou, M. Solomonow, A. Veicsteinas, *J. Electromyogr. Kinesiol.* **1999**, *9*, 131.
[15] B. J. Raiteri, A. G. Cresswell, G. A. Lichtwark, *PeerJ* **2016**, *4*, 2260.
[16] L. A. Hallock, A. Velu, A. Schwartz, R. Bajcsy, presented at 2020 8th IEEE RAS EMBS Int Conf Biomed Robotics Biomechatronics Biorob, IEEE, New York City, NY, December **2020**.

[17] J. Shi, Y. P. Zheng, Q. H. Huang, X. Chen, *IEEE Trans. Biomed. Eng.* **2008**, *55*, 1191.
[18] J. Y. Guo, Y. P. Zheng, H. B. Xie, X. Chen, *Med. Eng. Phys.* **2010**, *32*, 1032.
[19] X. Chen, YP. Zheng, JY. Guo, Z. Zhu, SC. Chan, Z. Zhang, *Eur. J. Appl. Physiol.* **2012**, *112*, 2603.
[20] R. Dahmane, V. Valenčič, N. Knez, I. Eržen, *Med. Biol. Eng. Comput.* **2001**, *39*, 51.
[21] S. Đorđević, S. Stančin, A. Meglič, V. Milutinović, S. Tomažič, *Sensors* **2011**, *11*, 9411.
[22] Z. G. Xiao, C. Menon, *Sensors* **2019**, *19*, 4557.
[23] J. T. Alvarez, L. F. Gerez, O. A. Araromi, J. G. Hunter, D. K. Choe, C. J. Payne, R. J. Wood, C. J. Walsh, *IEEE T Neur. Sys. Reh.* **2022**, *30*, 2198.
[24] A. Radmand, E. Scheme, K. Englehart, *J. Rehabil. Res. Dev.* **2016**, *53*, 443.
[25] J. Guo, C. Guo, J. Zhou, K. Duan, Q. Wang, *Soft Robot.* **2022**, *10*, 601.
[26] T. Wang, Y. Zhao, Q. Wang, *IEEE Trans. Biomed. Eng.* **2023**, *70*, 3401.
[27] J. Xu, T. Tat, J. Yin, D. Ngo, X. Zhao, X. Wan, Z. Che, K. Chen, L. Harris, J. Chen, *Matter* **2023**, *6*, 2235.
[28] N. Bu, J. Tsukamoto, N. Ueno, K. Shima, T. Tsuji, presented at 2008 30th Annual Int. Conf. IEEE Eng. Med. Biol. Soc., IEEE, BC, Canada, August **2008**, 112.
[29] L. F. Gerez, J. T. Alvarez, E. Debette, O. A. Araromi, R. J. Wood, C. J. Walsh, IEEE, Singapore, September **2023**.
[30] C. Orizio, M. Gobbo, A. Veicsteinas, R. V. Baratta, B. H. Zhou, M. Solomonow, *Eur. J. Appl. Physiol.* **2003**, *88*, 601.
[31] V. Valenčič, N. Knez, *Artif. Organs* **1997**, *21*, 240.
[32] J. S. Schofield, K. R. Evans, J. S. Hebert, P. D. Marasco, J. P. Carey, *J. Biomech.* **2016**, *49*, 786.
[33] H. Wang, S. Zuo, M. Cerezo-Sánchez, N. G. Arekhloo, K. Nazarpour, H. Heidari, *Front. Neurosci.* **2022**, *16*, 1020546.
[34] M. Wininger, *J. Rehabil. Res. Dev.* **2008**, *45*, 883.
[35] B. Simunic, D. Krizaj, M. Narici, R. Pisot, *Ann. Kinesiologiae* **2010**, *1*.
[36] S. Đorđević, S. Tomažič, M. Narici, R. Pišot, A. Meglič, *Sensors* **2014**, *14*, 17848.
[37] R. G. P. Lopata, J. P. van Dijk, S. Pillen, M. M. Nillesen, H. Maas, J. M. Thijssen, D. F. Stegeman, C. L. de Korte, *J. Appl. Physiol.* **2010**, *109*, 906.
[38] X. Yang, Y. Li, Y. Fang, H. Liu, presented at 2017 8th Int. IEEE EMBS Conf. Neural. Eng. (NER), IEEE, Shanghai, China, May **2017**, 118.
[39] B. J. Raiteri, A. G. Cresswell, G. A. Lichtwark, *Proc. Natl. Acad. Sci.* **2018**, *115*, E3097.
[40] C. J. Arellano, N. J. Gidmark, N. Konow, E. Azizi, T. J. Roberts, *J. Biomech.* **2016**, *49*, 1812.
[41] C. Schwiete, C. Roth, C. Braun, L. Rettenmaier, K. Happ, G. Langen, M. Behringer, *PLoS One* **2023**, *18*, 0281651.
[42] L. A. Hallock, A. Kato, R. Bajcsy, presented at 2018 IEEE Int. Conf. Rob. Autom. (ICRA), IEEE, Brisbane, QLD, Australia, May **2018**, 1825.
[43] C. Latella, C. V. Ruas, R. N. O. Mesquita, K. Nosaka, J. L. Taylor, *J. Electromyogr. Kinesiol.* **2019**, *45*, 26.
[44] B. Šimunič, *J. Biomech.* **2019**, *92*, 92.
[45] K. Koren, E. Rejc, B. Simunic, S. Lazzer, *Kineziologija* **2015**, *47*, 19.
[46] A. Kadkhodayan, X. Jiang, C. Menon, *J. Med. Biol. Eng.* **2016**, *36*, 594.
[47] J. A. Majdi, S. A. Acuña, P. V. Chitnis, S. Sikdar, *Wearable Technol.* **2022**, *3*, 16.
[48] E. Cè, S. Longo, E. Limonta, G. Coratella, S. Rampichini, F. Esposito, *Eur. J. Appl. Physiol.* **2020**, *120*, 17.
[49] A. M. Hunter, S. D. Galloway, I. J. Smith, J. Tallent, M. Ditroilo, M. M. Fairweather, G. Howatson, *J. Electromyogr. Kinesol.* **2012**, *22*, 334.
[50] B. Šimunič, Doctoral Thesis, University of Ljubljana, Ljubljana **2003**.
[51] D. McAndrew, M. Gorelick, J. M. M. Brown, *J. Musculoskeletal Res.* **2006**, *10*, 23.
[52] R. M. Enoka, I. G. Amiridis, J. Duchateau, *Physiology* **2020**, *35*, 40.
[53] B. Ravary, P. Pourcelot, C. Bortolussi, S. Konieczka, N. Crevier-Denoix, *Clin. Biomech.* **2004**, *19*, 433.
[54] C. R. Taylor, S. S. Srinivasan, S. H. Yeon, M. K. O'Donnell, T. J. Roberts, H. M. Herr, *Sci. Rob.* **2021**, *6*, eabg0656.
[55] T. J. Roberts, R. L. Marsh, P. G. Weyand, C. R. Taylor, *Science* **1997**, *275*, 1113.
[56] J. Shi, Y. P. Zheng, X. Chen, Q. H. Huang, *Med. Eng. Phys.* **2007**, *29*, 472.
[57] L. J. Macgregor, M. Ditroilo, I. J. Smith, M. M. Fairweather, A. M. Hunter, *J. Sport Rehabilitation* **2016**, *25*, 241.
[58] R. Dahmane, S. Djordjevič, B. Šimunič, V. Valenčič, *J. Biomech.* **2005**, *38*, 2451.
[59] L. J. Macgregor, A. M. Hunter, C. Orizio, M. M. Fairweather, M. Ditroilo, *Sports Med.* **2018**, *48*, 1607.
[60] A. Liu, S. Araromi, C. J. Walsh, R. J. Wood, presented at 2023 IEEE Int. Conf. Rob. Autom. (ICRA), London, United Kingdom, June **2023**.
[61] H. Liu, H. Zhao, S. Li, J. Hu, X. Zheng, R. Li, Y. Chen, Y. Su, *Adv. Mater. Technol.* **2019**, *4*, 1800327.
[62] S. Lin, W. Yang, X. Zhu, Y. Lan, K. Li, Q. Zhang, Y. Li, C. Hou, H. Wang, *Nat. Commun.* **2024**, *15*, 2374.
[63] A. Meglič, M. Uršič, A. Škorjanc, S. Đorđević, G. Belušič, *Sensors* **2019**, *19*, 2108.
[64] D. Shah, S. J. Woodman, L. Sanchez-Botero, S. Liu, R. Kramer-Bottiglio, *Adv. Intell. Syst.* **2023**, *5*, 202300343.
[65] R. B. Woodward, S. J. Shefelbine, R. Vaidyanathan, *IEEE ASME Trans. Mechatron.* **2016**, *22*, 2022.
[66] Y. Lu, Y. Cao, Y. Chen, H. Li, W. Li, H. Du, S. Zhang, S. Sun, *Smart Mater. Struct.* **2023**, *32*, 065013.
[67] D. Esposito, G. D. Gargiulo, N. Parajuli, E. Andreozzi, P. Bifulco, presented at *2020 IEEE Int. Symp. Med. Meas. Appl. (MeMeA)*, IEEE, Bari, Italy, October **2020**, pp. 1–6. https://doi.org/10.1109/MeMeA49120.2020.9137313.
[68] P. Chen, Z. Li, S. Togo, H. Yokoi, Y. Jiang, presented at *IEEE Trans. Hum.-Mach. Syst IEEE*, IEEE, October **2023**, *53*, pp. 935–944.
[69] S. Frey, V. Kartsch, C. Leitner, A. Cossettini, S. Vostrikov, S. Benatti, L. Benini, presented at 2023 IEEE Int. Ultrason. Sympos. (IUS), IEEE, Montreal, QC, Canada, September **2023**.
[70] C. Calvo-Lobo, I. Díez-Vega, M. García-Mateos, J. J. Molina-Martín, G. Díaz-Ureña, D. Rodríguez-Sanz, *Rev. da Assoc. Médica Bras.* **2017**, *64*, 549.
[71] A. M. Alfuraih, A. Alhowimel, S. Alghanim, Y. Khayat, A. Aljamaan, H. I. Alsobayel, *Sensors* **2022**, *22*, 1206.
[72] T. J. M. Dick, J. M. Wakeling, *J. Appl. Physiol.* **2017**, *123*, 1433.
[73] T. J. M. Dick, A. A. Biewener, J. M. Wakeling, *J. Exp. Biol.* **2017**, *220*, 1643.
[74] M. Ditroilo, I. J. Smith, M. M. Fairweather, A. M. Hunter, *J. Electromyogr. Kinesiol.* **2013**, *23*, 558.
[75] K. N. An, K. R. Kaufman, E. Y. S. Chao, *J. Biomech.* **1989**, *22*, 1249.
[76] G. Langen, I. Sandau, O. Ueberschär, K. Nosaka, M. Behringer, J. Electromyogr Kines **2022**, *67*, 102702.
[77] E. Kreyszig, *Differential Geometry*, Dover Publications, Mineola, New York **1990**.
[78] J. D'Errico, Arclength, Natick, Massachusetts, **2023**.
[79] R: A Language and Environment for Statistical Computing, R Foundation For Statistical Computing, Vienna, Austria, **2023**.